Raman study of CeO_2: Second-order scattering, lattice dynamics, and particle-size effects

W. H. Weber, K. C. Hass, and J. R. McBride
Physics Department, Research Laboratory, MD-3028/SRL, Ford Motor Company, Dearborn, Michigan 48121-2053
(Received 30 November 1992)

Polarized Raman-scattering spectra are obtained from oriented single crystals of CeO_2. Second-order features are assigned to phonon overtones from the X and L points on the Brillouin-zone boundary on the basis of selection rules and by analogy to another fluorite structure compound, BaF_2, in which the phonon dispersion curves are known. Complete selection rules for second-order scattering from these high-symmetry points are determined. A rigid-ion model is constructed for the phonon dispersion curves by fitting several of these features and the known zone-center optical modes. The F_{2g} Raman-active mode at 465 cm^{-1} in CeO_2 shifts and broadens with decreased particle size [G. W. Graham, W. H. Weber, C. R. Peters, and R. Usmen, J. Catalysis **130**, 310 (1991)]. It is shown using the calculated dispersion curves that this particle-size effect cannot be explained with the spatial-correlation model.

I. INTRODUCTION

Cerium dioxide, CeO_2, and several other f-electron metal dioxides (ThO_2 and UO_2) crystallize in the fluorite-structure lattice (space group O_h^5). This structure has six optical-phonon branches, which yield three zone-center frequencies. In CeO_2 these frequencies are 272, 465, and 595 cm^{-1}, corresponding to the doubly degenerate TO mode, the triply degenerate Raman-active mode, and the nondegenerate LO mode, respectively. The Raman mode frequency is given directly by the Raman measurements,[1,2] whereas the TO and LO frequencies are given indirectly by fits to infrared reflectivity.[2,3] There have been no neutron-scattering studies of CeO_2, and thus there is no experimental information on the phonon dispersion curves away from the zone center. The primary goal of this work is to provide new information about these curves in CeO_2 through a study of the second-order Raman spectrum. In principle, this spectrum is quite complicated, since it involves considering all allowed pairs of phonons from as many as nine different branches throughout the Brillouin zone. In practice, however, it has been found that in many compounds (e.g., Si,[4] Ge,[4] PdO,[5] and diamond[6]) the simple overtone density of states (DOS), i.e., the one-phonon DOS with the frequency scale multiplied by two, correlates well with the observed second-order spectrum. This means that features in the second-order spectrum usually correspond to overtones of phonon modes at critical points in $\mathbf{k}$ space, which are often high-symmetry points on the Brillouin-zone boundary. We will see here, by first examining the case of BaF_2, that this correspondence is less complete in ionic fluorite-structure compounds than in the more covalent materials mentioned above. Nevertheless, the second-order Raman spectrum for CeO_2 provides several constraints that allow us to construct a more satisfactory model of the phonon-dispersion curves in this compound than has been given previously.[7]

Krishnamurthy and Soots[8] have given a detailed theoretical analysis of second-order scattering in fluorite-structure crystals, along with experimental results on several fluorides. They assign numerous features in the second-order spectra, but their calculated joint two-phonon DOS spectra generally show only fair agreement with experiment. In addition, their theoretical analysis contains several errors, since it is based on an earlier paper by Ganesan and Burstein,[9] who incorrectly labeled the symmetries of the zone-boundary phonons. The only previous experimental study of second-order scattering in CeO_2 was by Kourouklis, Jayaraman, and Espinosa,[10] who made tentative assignments using spectra obtained from unoriented crystals in a diamond-anvil cell.

The paper is organized as follows: In Sec. II we present experimental results on the crystal growth and on polarized Raman scattering from oriented CeO_2 crystals. In Sec. III we give a calculation of the phonon-dispersion curves for CeO_2 along with a comparison between the second-order spectra and the overtone DOS's for both BaF_2 and CeO_2. We also give the selection rules for second-order scattering from phonons at the X and L points on the Brillouin-zone boundary, correcting the errors in previous studies.[8,9] In Sec. IV we discuss the particle-size effect in the CeO_2 Raman spectra recently reported by Graham *et al.*[11] and show that it cannot be explained using the spatial-correlation model.[12,13] This model is often invoked to interpret size effects, and to implement it we use the dispersion curves obtained in Sec. III. A brief summary is given in Sec. V.

II. EXPERIMENTAL RESULTS

The CeO_2 crystals were grown by Wanklyn and Garrard[14] using a flux method in solutions of $PbO+PbF_2$. Two types of crystals were studied: clear brownish crystals that grew with a platelike habit and had facets several mm on a side and clear bluish crystals that were more cubical in shape and somewhat smaller. The two crystal types resulted from different starting compositions and slightly different thermal treatments.[14]

The Raman spectra were obtained with an Ar-ion laser

and an array detector system described in more detail elsewhere.[5] The spectra from the two types of crystals were nearly identical, except for weak fluorescence lines arising from impurities. Consequently, we will show only results from the larger, brown crystals. Polarized Raman spectra, shown in Fig. 1, were obtained from a crystal having a large (001) surface with (100) and (010) edges, as determined by Laue back-reflection x-ray analysis. The laser beam was incident on the crystal s polarized at $\sim 65°$ from the normal, i.e., from the (001) direction, and the scattered light was collected normal to the surface with an $f/1.4$ camera lens. The spectra are labeled by the directions of the incoming and outgoing electric vectors and by the symmetries of the scattering tensors that would be observed in each case. We use the Mulliken notation for these symmetries; the notation of Ref. 8 can be obtained by the transformation $A_{1g} \rightarrow \Gamma^{(1+)}$, $E_g \rightarrow \Gamma^{(12+)}$, and $F_{2g} \rightarrow \Gamma^{(25+)}$. The x and y axes correspond to the cubic crystal axes; x' and y' are rotated from these by 45° about z. The 488-nm laser line was used, since it produced no observable fluorescence in this crystal in the spectral region of interest. These spectra are corrected for the polarization dependence of the spectrometer throughout. Thus, relative intensities at the same Raman shift can be directly compared amongst the different spectra.

The primary feature in Fig. 1 is the first-order-allowed Raman line at 465 cm^{-1}, which has F_{2g} symmetry and completely dominates the $x'x'$ and xy spectra. Because of polarization leakage, this line also dominates the xx and $x'y'$ scattering configurations, for which it is forbidden. The second-order features, of which seven can be identified, are most prominent in the xx geometry. As shown in the figure, these have primarily A_{1g} symmetry, with the features near 600 and 1180 cm^{-1} having small additional contributions from E_g and F_{2g} symmetries, respectively. In the blue crystals the weak broad line near 935 cm^{-1} was weaker by a factor ~ 3 relative to the other structure. Otherwise the Raman spectra from the two types of crystals were identical.

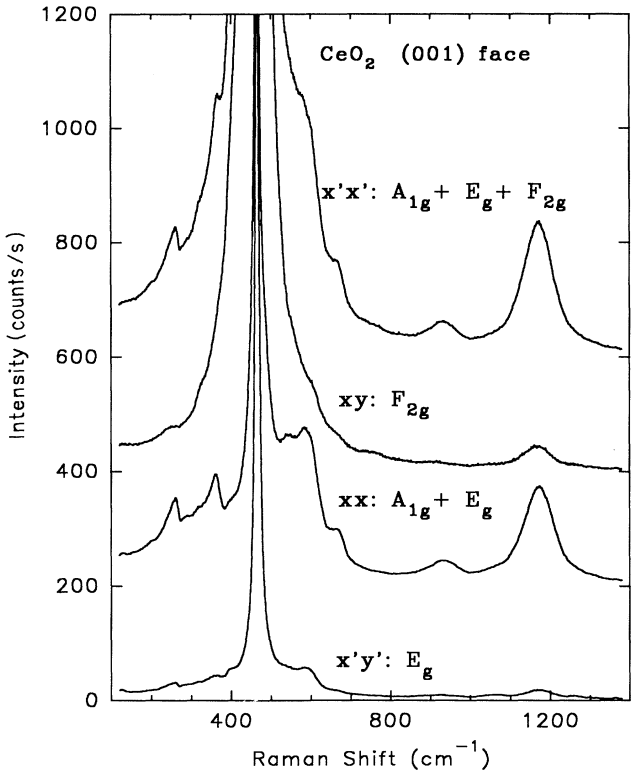

FIG. 1. Polarized Raman spectra from a CeO_2 single crystal obtained with the 488-nm Ar-ion laser line. The scale for the $x'y'$ spectrum is labeled on the left; that for subsequent spectra is shifted up by one tic mark (200 counts/s).

TABLE I. Second-order Raman features in CeO_2.

Observed features (cm^{-1})	Assignments and phonon symmetries[a]	Scattering tensors
264	$2TA(L)-L_3' \times L_3'$	A_{1g},E_g,F_{2g}
366	$2TA(X)-X_5' \times X_5'$	A_{1g},E_g,F_{2g}
550	$2LA(L)-L_1' \times L_1'$	A_{1g},F_{2g}
	$2LA(X)-X_2' \times X_2'$	A_{1g},E_g
600	$2TO(X)-X_5 \times X_5$	A_{1g},E_g,F_{2g}
676	$2LO_R(X)-X_3' \times X_3'$	A_{1g},E_g
935	$2TO_R(X)-X_5' \times X_5'$	A_{1g},E_g,F_{2g}
1180	2LO	

[a]Symmetries for the phonons and scattering tensors from Tables II and IV.

Our assignments for the second-order features are given in Table I. These are motivated in Sec. III by results for other fluorite-structure compounds, a lattice-dynamical model for CeO_2, and an analysis of selection rules for two-phonon combinations.

III. THEORETICAL ANALYSIS

A. Lattice-dynamics model

To our knowledge, the only existing calculation of the phonon-dispersion curves in CeO_2 is that of Sato and Tateyama.[7] These authors employed a rigid-ion model (RIM) with parameters fit to assumed values for the zone-center frequencies and elastic constants. This model has a major deficiency in that it was based on a zone-center LO mode frequency of 750.3 cm^{-1}, instead of the presently accepted experimental value[2,3] of 595 cm^{-1}. The elastic constants used in this model are also suspect, since they were simply assumed to be the same as in ThO_2; Sato and Tateyama[7] cite an unpublished verification of this assumption for the compressibility, but independent measurements of c_{11}, c_{12}, and c_{44} in CeO_2 have yet to be performed.

Much more information is available for the phonon-dispersion curves in other fluorite-structure compounds.[15] The basic RIM approach to this problem was outlined by Srinivasan[16] in 1958. The next two decades saw a flurry of activity in which the phonon spectra of UO_2,[17] CaF_2,[18] and many other fluorite-structure compounds[15] were measured directly by inelastic neutron

scattering. Concurrently, the shell model,[19] which relaxes the constraint that the ionic charge be rigidly attached to the nucleus, emerged as the method of choice for describing phonons in ionic compounds. Least-squares fits to the neutron data showed the shell model to be far superior to the RIM for providing global descriptions of the phonon spectra of fluorite-structure compounds.[15] The RIM is often adequate for the acoustic and lower optic branches, but it is generally qualitatively incorrect for the highest, LO phonon branch. The shell model, of course, has its own drawback in that it introduces additional parameters that are difficult to constrain in materials such as CeO_2 that have not been studied by inelastic neutron scattering.

Useful insights into the general behavior of fluorite-structure compounds may be obtained by considering the prototypical case of BaF_2 . Figure 2 shows the phonon-dispersion curves for this compound as calculated from the 11-parameter shell model of Hurrell and Minkiewicz.[20] The symmetry labels in Fig. 2 were carefully determined from the displacement patterns for individual eigenstates. We follow here the notation of Koster[21] (also used by Dolling, Cowley, and Woods[17,22]) with the minor modification that we label the symmetries at the X point of the fcc Brillouin zone by X's instead of M's. For the fluorite structure, with O_h^5 space group, the eigenstates at X and at L and along the (100), (110), and (111) directions in **k** space correspond to irreducible representations of the groups D_{4h}, D_{3d}, C_{4v}, C_{2v}, and C_{3v}, respectively.[23] Table II lists the frequencies of the phonons at Γ, X and L in the shell model for BaF_2 and shows the correspondence between the present Koster notation[21] and two other commonly used sets of symmetry labels.[23,24] It will be important later on to note that all of the modes at these high-symmetry points are either even or odd with respect to inversion (g or u, respectively, in the Mulliken notation). Ganesan and Burstein,[9] in an early analysis of phonon states in fluorite-structure crystals, used the Loudon notation,[24] but incorrectly identified the symmetries of individual modes. As already mentioned in Sec. I, Krishnamurthy and Soots[8] based their own work on the symmetries of two-phonon combinations on these incorrect

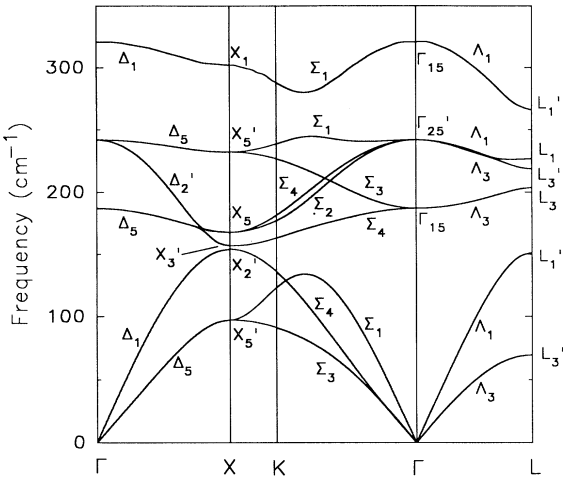

FIG. 2. Phonon-dispersion curves for BaF_2 calculated using the shell model of Ref. 20.

TABLE II. Calculated frequencies and symmetry designations for phonons in fluorite-structure crystals at Γ, X, and L.

Group of **k**	Frequency (cm^{-1})[a] CeO_2	BaF_2	Description	Representation Koster notation Ref. 21	Mulliken notation Ref. 23	Loudon notation Ref. 24
$\Gamma:O_h$	0	0	TA,LA	Γ_{15}	F_{1u}	Γ_{15}^-
	272	187	TO	Γ_{15}	F_{1u}	Γ_{15}^-
	595	321	LO			
	464	242	R	Γ'_{25}	F_{2g}	Γ_{25}^+
$X:D_{4h}$	183	97	TA	X'_5	E_u	X_5^-
	272	154	LA	X'_2	A_{2u}	X_4^-
	295	168	TO	X_5	E_g	X_5^+
	341	157	LO_R	X'_3	B_{1u}	X_2^-
	475	232	TO_R	X'_5	E_u	X_5^-
	559	302	LO	X_1	A_{1g}	X_1^+
$L:D_{3d}$	132	70	TA	L'_3	E_u	L_3^-
	268	151	LA	L'_1	A_{1u}	L_1^-
	378	204	TO	L_3	E_g	L_3^+
	384	219	TO_R	L'_3	E_u	L_3^-
	491	227	LO_R	L_1	A_{1g}	L_1^+
	504	266	LO	L'_1	A_{1u}	L_1^-

[a]Frequencies for BaF_2 and CeO_2 are calculated using the shell model of Ref. 20 and the rigid-ion model described in the text, respectively.

assignments.

The shell model parameters for BaF_2 were fit to neutron-scattering measurements.[20] The resulting dispersion curves are in excellent agreement with the data for all but the highest branch, which is too low in Fig. 2 by about 10%. The qualitative features of the phonon spectra are similar in all fluorite-structure compounds.[15] The BaF_2 Raman mode lies at 242 cm^{-1} and the zone-center TO and LO modes in the shell model lie at 187 and 321 cm^{-1}, respectively.

Figure 3 compares the overtone DOS calculated for this model with a polarized Raman spectrum measured in our laboratory for an oriented single crystal of BaF_2 in the xx scattering configuration. As in Fig. 1, the strong line at 242 cm^{-1} is the Raman-active mode and should be ignored since it arises from polarization leakage. The remaining features have primarily A_{1g} symmetry and are due to second-order scattering. Vertical lines have been drawn at calculated overtone frequencies from X- or L-point phonons that appear to correlate with observed structure. The strongest correlation is with the lowest-frequency peak labeled 2TA(L). Several phonons at X appear to contribute to the peak near 330 cm^{-1}. The peak near 370 cm^{-1} does not correspond to a zone-boundary phonon overtone, but it does match a peak in the 2ω DOS. The correlation between the 2LO band and the observed spectrum is quite good considering that the calculated band should be shifted up by $\sim 10\%$ to fit the

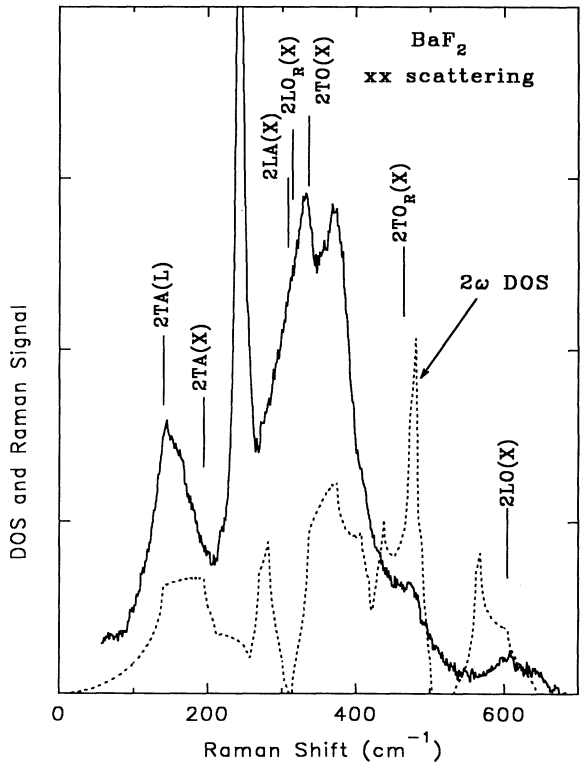

FIG. 3. Polarized Raman spectrum from an oriented single crystal of BaF_2 (solid curve) and overtone DOS from the shell model calculation in Fig. 2 (dashed curve).

neutron-scattering data.[20] We conclude that features in the second-order spectrum correlate with the overtone frequencies of phonons from various high-symmetry points, even though the relative intensities of these features are not given well by the overtone DOS.

The above experience with BaF_2 will now prove valuable as we construct a model of the lattice dynamics of CeO_2. Although a shell model would be preferable in principle, the available experimental information for CeO_2 is too limited at present to constrain such a model adequately. We will therefore consider only a RIM description and will correct later for its most glaring deficiency.

There are six constraints that we impose on the model. The first three are that it give the correct frequencies for the zone-center TO, LO, and Raman modes. We also require that the model reproduce the experimental compressibility, which is ensured by fitting the bulk modulus $[(c_{11}+2c_{12})/3]$ to its value in Ref. 7. Finally, we fit the TA mode frequencies at X and L to the values 183 and 132 cm^{-1}, respectively. This last constraint follows from the assumption that it is the overtones of these modes that are responsible for the observed peaks in the second-order Raman spectrum of CeO_2 at 366 and 264 cm^{-1} in Fig. 1.

To satisfy these constraints, we employ a six-parameter RIM that is a slight generalization of those of Srinivasan[16] and Sato and Tateyama.[7] The six parameters are Z_c, the effective charge on the Ce, and the near-neighbor force constants, A_1, B_1, A_2, B_2, and A_3. The short-range interactions are assumed to be axially symmetric, with A the radial component and **B** the tangential component. The subscripts 1, 2, and 3 denote Ce-O, O-O, and Ce-Ce nearest neighbors, respectively. Many analytic results for this and more general RIM's for fluorite-structure crystals may be found in the literature.[7,16–18] We will not reproduce these results here but we have used them to impose our constraints. With $r_0=2.7$ Å as the value of the half lattice constant, we obtain the RIM parameters for CeO_2 listed in Table III. Also listed are the individual elastic constants predicted by this model, which differ from the values assumed by Sato and Tateyama.[7] The calculated eigenvalues at Γ, X, and L are given in Table II.

The new RIM yields the phonon-dispersion curves for CeO_2 shown in Fig. 4. As anticipated, the qualitative features are very similar to those in Fig. 2 for BaF_2, although the CeO_2 curves extend about twice as high in frequency, indicative of significantly stronger bonding. (The masses are nearly identical in the two cases.) Another difference between the two cases is that the splitting between the two highest Σ_1 branches in Fig. 4 is practically nonexistent, whereas the uppermost branch is well separated in Fig. 2. A poor description of this uppermost LO phonon branch is a well-known deficiency of the RIM for ionic crystals.[15] At lower frequencies, the present model for CeO_2 is expected to be reasonably reliable. In this regime, the results in Fig. 4 are not that different (typically <30 cm^{-1}) from those of Sato and Tateyama.[7] One slightly unusual prediction of both of

TABLE III. Rigid-ion model parameters and calculated elastic constants for CeO_2.

RIM parameters					
Effective charge		Force constants (10^5 dyn/cm)		Elastic constants (10^{12} dyn/cm)	
Z_c	2.412	A_1	1.361	c_{11}	3.106
		B_1	−0.200	c_{12}	1.093
		A_2	0.004	c_{44}	1.451
		B_2	0.091		
		A_3	0.254		

these models compared to results for BaF_2 and other fluorite crystals is that the Δ_2' branch does not disperse strongly enough to cross the Δ_5 branch that connects to the TO mode at Γ. The dispersion of the Δ_2' branch is a sensitive function of the parameters, and it is thus possible that the lack of crossing in CeO_2 is an artifact. We will return to this point in the discussion of the spatial correlation model in the next section.

Figure 5 shows the total one-phonon DOS for the present CeO_2 model together with the projections of this spectrum on O and Ce sites. Because of the large mass difference between Ce and O, the low-frequency vibrations are dominated by the motion of the heavy Ce ions, while the higher-frequency vibrations are almost entirely due to O. There is a pronounced dip in the DOS near 500 cm^{-1}, which corresponds to the small gap between the upper two Σ_1 branches in Fig. 4. Since we know that the upper branch is unreliable in the RIM, the existence of this dip suggests a simple way of "improving" the present model by rigidly shifting the portion of the DOS above this dip to higher frequencies. Such a shift is analogous to the so-called "scissor" operation that is often employed in density-functional theory calculations to correct for the underestimate of electronic band gaps.[25] It should be noted that the present correction is intended primarily for the DOS itself and that the actual dispersion curve for the highest branch in CeO_2 cannot be realistically modeled by such a shift, since the zone-center LO frequency is already correct in Fig. 4. In a future publication, we will show that by improving the DOS in this manner, we obtain better agreement between theory and experiment for the effects of O vacancies in CeO_2. A more important justification for the proposed shift is provided by the second-order Raman measurements, as discussed below.

B. Second-order scattering, selection rules, and comparisons with experiment

It is useful at this point to derive the symmetries of the Raman tensors for second-order scattering from zone-boundary phonons at X and L. (Phonons at Γ are generally less important in second-order scattering because they are usually not associated with a large DOS.) We have already listed the symmetries of the individual phonon modes at X and L in Table II. We must next determine the irreducible representations of the binary com-

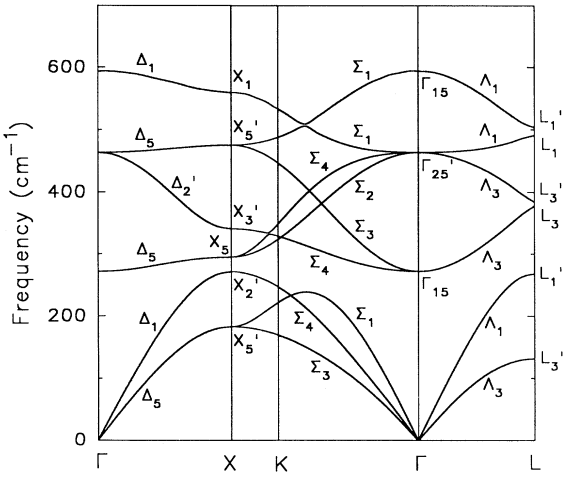

FIG. 4. Phonon-dispersion curves for CeO_2 calculated using the rigid-ion model described in the text.

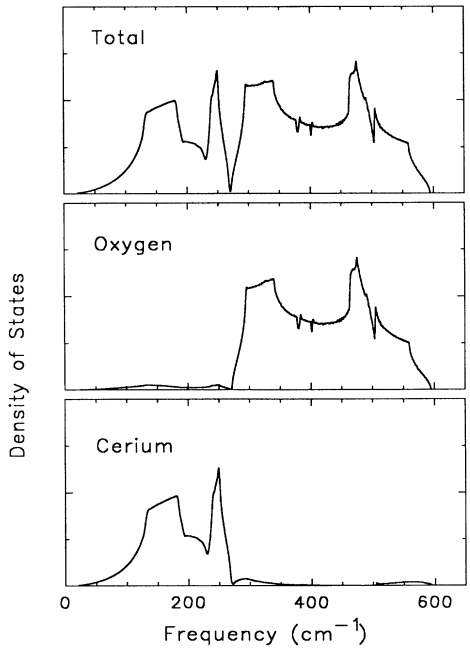

FIG. 5. Total and projected density of states for model of Fig. 4.

binations at each of these points. This is accomplished by simply multiplying together the characters of the individual group operations.[26] The final step is to establish the correlations between the irreducible representations of the combinations in the group of a particular **k** and the irreducible representations of the full space group. The general procedure for working out these correlations is given by Turrell.[23] Results for the O_h^5 space group have been tabulated previously by Loudon[24] and others.[23,27] For a binary combination to be Raman active, it must correlate with at least one of the three Raman-active symmetries: A_{1g}, E_g, or F_{2g}. Table IV lists all the Raman-allowed combinations with their scattering tensors. Since parity is a good quantum number at X and L, only combinations with the same inversion symmetry (g or u) are Raman allowed.

Figure 6 shows the xx Raman spectrum of CeO_2 with the calculated positions of the assignments given in Table I indicated by vertical lines. Note that having constrained the TA mode to fit the two lowest frequency peaks at L and X, the remaining structure in the spectrum lines up fairly well with other phonon overtones, which is the primary justification for the assignments given in the table. The peak near 1180 cm^{-1} is so broad and symmetrical that it makes no sense to assign it to a single critical point phonon overtone; rather, we label this peak simply as 2LO.

The dashed curve in Fig. 6 is the overtone DOS derived from the model of Figs. 4 and 5 in which the uppermost portion of the one-phonon spectrum has been shifted by 60 cm^{-1}. It is clear that without a shift of roughly this magnitude, it would be difficult to account for the large second-order Raman peak near 1180 cm^{-1}.

Kourouklis, Jayaraman, and Espinosa[10] have reported second-order features in CeO_2 (580, 660, 880, 1030, and 1160 cm^{-1}) with tentative assignments of their possible origins based on the dispersion curves calculated by Sato and Tateyama.[7] Of these, only the features at 580, 660, and 1160 cm^{-1} correspond to structure seen in our spectra. They assign the 580-cm^{-1} feature to $TO(X)+LA(X)$, which must be in error, since this combination has $X_5 \times X_2'$ symmetry and is Raman forbidden (by parity). The 660-cm^{-1} line is assigned to $\omega_R(X)+LA(X)$ which is ambiguous, since the Raman mode at X splits into LO and TO components with quite different frequencies. The former would lead to a combination symmetry of $X_3' \times X_2'$, the latter to $X_5' \times X_2'$. In either case the resulting scattering tensor (see Table IV) is F_{2g}, which is inconsistent with the observation that all the features have primarily A_{1g} symmetry. Their assignment of the 1160-cm^{-1} line to 2LO is consistent with our assignment of the 1180-cm^{-1} feature.

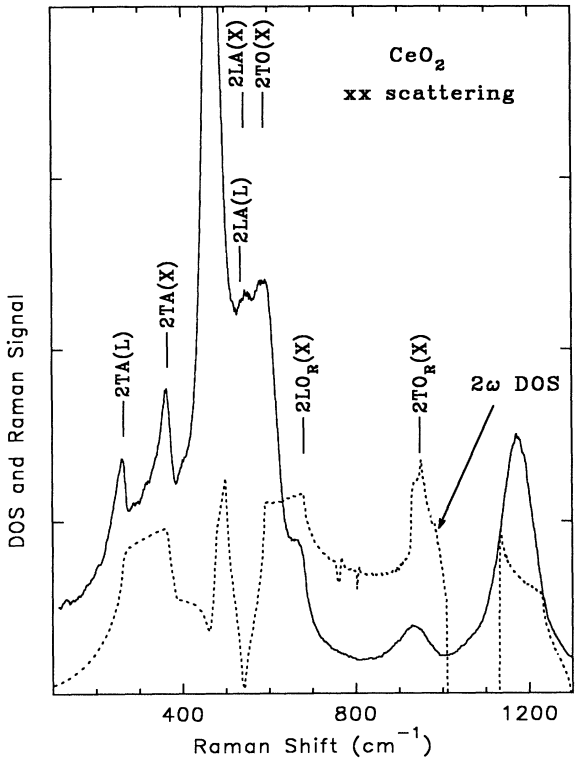

FIG. 6. Polarized Raman spectrum of CeO_2 from Fig. 1 (solid curve), with assignments from Table I given by vertical lines, and calculated overtone DOS with the highest frequency LO band shifted as described in the text (dashed curve).

TABLE IV. Raman-active combinations and scattering tensors for second-order processes from phonons at X and L in fluorite-structure crystals.

Phonon combinations	Scattering tensors
$X_1 \times X_1$	A_{1g}, E_g
$X_2' \times X_2'$	A_{1g}, E_g
$X_3' \times X_3'$	A_{1g}, E_g
$X_5' \times X_5'$	A_{1g}, E_g, F_{2g}
$X_5 \times X_5$	A_{1g}, E_g, F_{2g}
$X_1 \times X_5$	F_{2g}
$X_3' \times X_5'$	F_{2g}
$X_2' \times X_5'$	F_{2g}
$X_2' \times X_3'$	F_{2g}
$L_1 \times L_1$	A_{1g}, F_{2g}
$L_1' \times L_1'$	A_{1g}, F_{2g}
$L_3 \times L_3$	A_{1g}, E_g, F_{2g}
$L_3' \times L_3'$	A_{1g}, E_g, F_{2g}
$L_1 \times L_3$	E_g, F_{2g}
$L_1' \times L_3'$	E_g, F_{2g}

IV. PARTICLE-SIZE EFFECTS

Graham *et al.*[11] have noted systematic changes in the Raman spectrum of CeO_2 when the crystallite size, as determined by x-ray analysis, decreases down to ~70 Å. The Raman-allowed mode shifts very slightly to lower frequency (by a few cm^{-1}) but it shows a substantial broadening. We have continued these studies to even smaller particles using powdered samples obtained by first drying and then sintering at 900 °C aqueous solutions of cerium nitrate. Figure 7 shows our results combined with those of Ref. 11 for the variation of the half-width of the Raman line as a function of the inverse crystallite

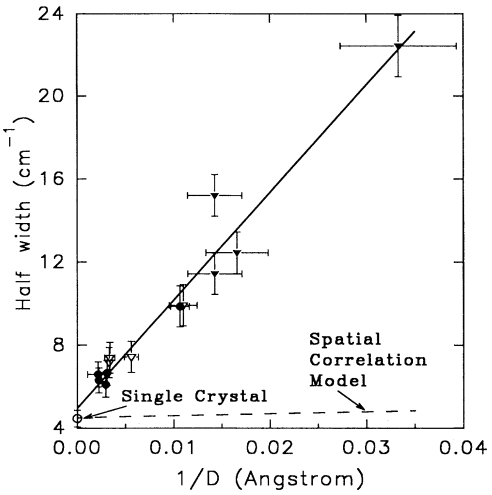

FIG. 7. Observed variation of the Raman linewidth in CeO_2 vs particle size (data points). Different symbols correspond to different preparation techniques. The solid line is a linear least-squares fit and the dashed line is the spatial-correlation model described in the text.

size. The particle sizes were obtained from x-ray analyses as described in Ref. 11, and the Raman linewidths by a least-squares fit of each spectrum to a Lorentzian line shape. The solid straight line is a linear least-squares fit to the form $\Gamma = a + b/D$, which yields $\Gamma(\text{cm}^{-1}) = 5 + 518/D(\text{Å})$.

Similar particle-size effects have been observed in Si,[12] GaAs,[13] CdSe,[28] Ge,[29] BN,[30] graphite,[31] and diamond.[32] In all of these studies attempts have been made to interpret the results using the spatial correlation model (also called the phonon confinement model).[12,13,33] A Gaussian correlation is usually assumed and the line shape is written in the form

$$I(\omega,\xi) = \frac{\xi^3}{\pi^{3/2}} \int d\mathbf{q} \frac{\exp(-\xi^2 q^2)}{[\omega - \omega(\mathbf{q})]^2 + \Gamma^2} , \quad (1)$$

where Γ is the half-width at half-maximum (HWHM) of the Raman line observed in a large single crystal (4.5 cm^{-1} for CeO_2) and ξ is the Gaussian correlation length, which would be proportional to the crystallite size. Various proportionality constants have been used by different authors, ranging from $\xi = D/2$ by Richter, Wang and Ley[12] to $\xi = D/4\pi$ by Campbell and Fauchet.[33] For a large crystal, i.e., $\xi \to \infty$, the integral in Eq. (1) contains $\delta(\mathbf{q})$, thus yielding a Lorentzian line centered at $\omega(0)$ with HWHM Γ.

We have evaluated Eq. (1) for the Raman mode of CeO_2 using the dispersion curves calculated in the previous section. Since the triple degeneracy of the Raman mode is removed at arbitrary points away from $q=0$, we sum Eq. (1) over the three equally weighted branches. The HWHM of the calculated line shapes is shown as the dashed line in Fig. 7, where we have chosen $\xi = D/2$. Clearly this theory fails to account for the magnitude of the observed broadening. Even if we allow for the fact that the dispersion of the Δ_2' branch in Fig. 4 might be underestimated, or if we chose the extreme case, $\xi = D/4\pi$, there is still an order of magnitude discrepancy in slope between theory and experiment. On the other hand, the spatial-correlation model does correctly predict the qualitative trends that as the particle-size decreases, the Raman peak shifts slightly to lower frequency and the line shape becomes asymmetric with a low-frequency tail.

A similar failure of the spatial-correlation model has been noted in BN, graphite, and diamond. In each case the qualitative features of the particle-size effects are given by the model, but the magnitude of the observed line broadening is much larger than predicted. Nemanich, Solin, and Martin[30] suggest that in BN the phonon lifetime reduction induced by surface and boundary scattering effects may contribute to the extra broadening. These effects might well be more pronounced for free-standing oxide particles, such as CeO_2, than for crystallites embedded in an amorphous matrix (e.g., Si and GaAs, as discussed in Ref. 33). Another possibility, suggested by Richter, Wang, and Ley,[12] is that the relaxation of strict momentum conservation in the anharmonic decay of the Raman mode into a pair of acoustic phonons with equal energy and opposite momenta may lead to a shorter lifetime. This possibility is attractive in CeO_2, since there is indeed a minimum in the DOS at roughly one half of the zone-center Raman mode frequency (~ 230 cm^{-1}, as seen in Fig. 5). Thus, relaxing momentum conservation will increase the decay rate of the Raman mode into a pair of acoustic phonons. To check this hypothesis, one must evaluate other possible two-phonon decay mechanisms, as done by Sato and Tateyama,[7] and then obtain combined temperature- and particle-size-dependent data to augment the data shown in Fig. 7. The broadening represented by Eq. (1) has no temperature dependence, whereas that associated with two-phonon decay would have a specific temperature dependence arising from the phonon occupation factors.

V. SUMMARY

In summary, we have obtained polarized Raman spectra from oriented single crystals of CeO_2 and assigned the observed structure to overtone scattering from phonons at X and L. These new assignments along with the known zone-center frequencies have allowed us to construct an improved rigid-ion model for the phonon-dispersion curves. The overtone DOS from this model correlates well with the observed spectra. A complete group-theoretic analysis is given for second-order scattering from the X and L points, and the observed selection rules for the assigned features are consistent with this analysis. The Raman-allowed line is found to shift and broaden as the particle size decreases, and we show that the broadening cannot be explained using the spatial-correlation model.

ACKNOWLEDGMENTS

We thank B. D. Poindexter for assistance in obtaining the Raman spectra and C. R. Peters for help with the x-ray analysis. We are indebted to B. M. Wanklyn from the Clarendon Laboratory, Oxford University, for providing the CeO_2 crystals.

[1]V. G. Keramidas and W. B. White, J. Chem. Phys. **59**, 1561 (1973).
[2]S. Mochizuki, Phys. Status Solidi B **114**, 189 (1982).
[3]F. Marabelli and P. Wachter, Phys. Rev. B **36**, 1238 (1987).
[4]M. Cardona, in *Light Scattering in Solids II,* edited by M. Cardona and G. Güntherodt, *Topics in Applied Physics,* Vol. 50 (Springer-Verlag, Berlin, 1982), pp. 62–69.
[5]J. R. McBride, K. C. Hass, and W. H. Weber, Phys. Rev. B **44**, 5016 (1991).
[6]K. C. Hass, M. A. Tamor, T. R. Anthony, and W. F. Banholzer, Phys. Rev. B **45**, 7171 (1992).
[7]T. Sato and S. Tateyama, Phys. Rev. B **26**, 2257 (1982).
[8]N. Krishnamurthy and V. Soots, Can. J. Phys. **50**, 849 (1972); **50**, 1350 (1972).
[9]S. Ganesan and E. Burstein, J. Phys. (Paris) **26**, 645 (1965).
[10]G. A. Kourouklis, A. Jayaraman, and G. P. Espinosa, Phys. Rev. B **37**, 4250 (1988).
[11]G. W. Graham, W. H. Weber, C. R. Peters, and R. Usmen, J. Catalysis **130**, 310 (1991).
[12]H. Richter, Z. P. Wang, and L. Ley, Solid State Commun. **39**, 625 (1981).
[13]K. K. Tiong, P. M. Amirtharaj, F. H. Pollak, and D. E. Aspnes, Appl. Phys. Lett. **44**, 122 (1984); P. Parayanthal and F. H. Pollak, Phys. Rev. Lett. **52**, 1822 (1984).
[14]B. M. Wanklyn and B. J. Garrard, J. Crys. Growth **66**, 346 (1984).
[15]W. Hayes and A. M. Stoneham, in *Crystals with the Fluorite Structure,* edited by W. Hayes (Clarendon, Oxford, 1974), Chap. 2, and references therein.
[16]R. Srinivasan, Proc. Phys. Soc. London **72**, 556 (1958).
[17]G. Dolling, R. A. Cowley, and A. D. B. Woods, Can. J. Phys. **43**, 1397 (1965).
[18]M. M. Elcombe and A. W. Pryor, J. Phys. C **3**, 492 (1970).
[19]For a review, see W. Cochran, Crit. Rev. Solid State Sci. **2**, 1 (1971).
[20]J. P. Hurrell and V. J. Minkiewicz, Solid State Commun. **8**, 463 (1970).
[21]G. F. Koster, in *Solid State Physics,* edited by F. Seitz and D. Turnbull (Academic, New York, 1957), Vol. 5, p. 173.
[22]Three phonon branches in Fig. 4 of Ref. 17 are mislabeled as Σ_3; they should be Σ_4. Appendix I of this reference, which is correct, contains a useful discussion of the compatibility relations for fluorite-structure crystals.
[23]See, for example, G. Turrell, *Infrared and Raman Spectra of Crystals* (Academic, New York, 1972), p. 297.
[24]R. Loudon, Proc. Phys. Soc. London **84**, 379 (1964).
[25]G. A. Baraff and M. Schlüter, Phys. Rev. B **33**, 7346 (1986).
[26]M. Tinkham, *Group Theory and Quantum Mechanics* (McGraw-Hill, New York, 1964), pp. 245–248.
[27]J. L. Birman, *Theory of Crystal Space Groups and Lattice Dynamics* (Springer-Verlag, Berlin, 1984), p. 440.
[28]A. Tanaka, S. Onari, and T. Arai, Phys. Rev. B **45**, 6587 (1992).
[29]M. Fujii, S. Hayashi, and K. Yamamoto, Appl. Phys. Lett. **57**, 2692 (1990).
[30]R. J. Nemanich, S. A. Solin, and R. M. Martin, Phys. Rev. B **23**, 6348 (1981).
[31]K. Nakamura, M. Fujitsuka, and M. Kitajima, Phys. Rev. B **41**, 12 260 (1990).
[32]J. W. Ager, D. K. Veirs, and G. M. Rosenblatt, Phys. Rev. B **43**, 6491 (1991).
[33]I. H. Campbell and P. M. Fauchet, Solid State Commun. **58**, 739 (1986).